Profiles of Low-Level Stratus Cloud Microphysics Deduced from Ground-Based Measurements

XIQUAN DONG* AND GERALD G. MACE

Meteorology Department, University of Utah, Salt Lake City, Utah

(Manuscript received 28 October 2001, in final form 16 June 2002)

ABSTRACT

The microwave radiometer–derived cloud liquid water path (LWP) and a profile of radar reflectivity are used to derive a profile of cloud liquid water content (LWC). Two methods (M1 and M2) have been developed for inferring the profile of cloud-droplet effective radius (r_e) in liquid phase or liquid dominant mixed phase stratocumulus clouds. The M1-inferred r_e profile is proportional to a previously derived layer-mean r_e and to the ratio of the radar reflectivity to the integrated radar reflectivity. This algorithm is independent of the radar calibration and is applicable to overcast low-level stratus clouds that occur during the day because it is dependent on solar transmission observations. In order to extend the retrieval algorithm to a wider range of conditions, a second method is described that uses an empirical relationship between effective radius and radar reflectivity based on theory and the results of M1. Sensitivity studies show that the surface-retrieved r_e is more sensitive to the variation of radar reflectivity when the radar reflectivity is large, and the uncertainties of retrieved r_e related to the assumed vertically constant cloud-droplet number concentration and shape of the size distribution are about 9% and 2%, respectively. For validation, a total of 10 h of aircraft data and 36 h of surface data were collected over the Atmospheric Radiation Measurement (ARM) program's Southern Great Plains (SGP) site during the March 2000 cloud intensive observational period (IOP). More detailed comparisons in two cases quantify the agreement between the aircraft data and the surface retrievals. When the temporal averages of the two datasets increase from 1 min to 30 min, the means and standard deviations of differences between the two datasets decrease from $-2.5\% \pm 84\%$ to $1.3\% \pm 42.6\%$ and their corresponding correlation coefficients increase from 0.47 to 0.8 for LWC; and decrease from $-4.8\% \pm 36.4\%$ to $-3.3\% \pm 22.5\%$ with increased coefficients from 0.64 to 0.94 for r_e (both M1 and M2). The agreement between the aircraft and surface data in the 30-min averages suggests that the two platforms are capable of characterizing the cloud microphysics over this temporal scale. On average, the surface retrievals are unbiased relative to the aircraft in situ measurements. However, when only the 1-min averaged aircraft data within 3 km of the surface site were selected, the means and standard deviations of differences between the two datasets are larger ($23.4\% \pm 113\%$ for LWC and $28.3\% \pm 60.7\%$ for r_e) and their correlation coefficients are smaller (0.32 for LWC and 0.3 for r_e) than those from all 1-min samples. This result suggests that restricting the comparison to the samples better matched in space and time between the surface and aircraft data does not result in a better comparison.

1. Introduction

Knowledge of the vertical structure of a cloud's microphysical characteristics is important for a variety of reasons. The profiles of cloud-droplet effective radius (r_e) and liquid water content (LWC) affect the cloud's interaction with solar and infrared radiation that ultimately contribute to the energy budget at the surface and top of atmosphere (TOA). Knowledge of the microphysical structure also increases our understanding of the process acting to form and maintain these cloud systems. This understanding may lead to improved numerical models and parameterizations of clouds. With the availability of cloud radar and other ground-based measurements from the Department of Energy Atmospheric Radiation Measurement (ARM) program (Stokes and Schwartz 1994), it is now possible to continuously monitor the vertical structure of clouds that occur over these sites and evaluate cloud properties in a statistical sense.

Several algorithms have been developed in recent years that combine millimeter wavelength radar (MMCR) observations with other data sources to derive the microphysical properties of low-level stratus clouds. The multiparameter algorithms developed for low-level liquid-phase stratus clouds use radar reflectivity observations and microwave radiometer–derived cloud liquid water path (LWP) combined with various assumptions to retrieve the microphysical properties of the cloud

* Current affiliation: Department of Atmospheric Sciences, University of North Dakota, Grand Forks, North Dakota.

Corresponding author address: Dr. Xiquan Dong, Department of Atmospheric Sciences, University of North Dakota, 4149 Campus Road, Clifford Hall 400, Box 9006, Grand Forks, ND 58202-9006.
E-mail: dong@aero.und.edu

layer. Since these techniques tend to assume a functional form (lognormal or gamma) for the particle size distribution, three independent parameters are generally needed to estimate the characteristics of the particle size distribution. These algorithms can be classified into those that use the solar transmission as additional independent information, such as Dong et al. (1997), Dong et al. (1998, hereafter D98) and Mace and Sassen (2000), and those that do not use the solar transmission but apply additional assumptions, such as Frisch et al. (1995, 1998, hereafter F95, F98, respectively). The solar transmission-based algorithms, because they use additional information, can be shown to be more accurate (Mace and Sassen 2000) but these algorithms can only be applied in a narrow range of conditions (daytime and overcast). Those algorithms that do not use solar transmission but use additional assumptions can be implemented more generally but tend to demonstrate larger error. Our goal in this study is to exploit the strengths of the two basic methodologies and develop a single framework that can be applied to continuous data without regard to the time of day or the existence of higher cloud layers.

2. Data

During March 2000, the ARM program conducted an intensive observational period (IOP) at the ARM Southern Great Plains (SGP; 36.61°N, 97.5°W) site to obtain comprehensive ground-based measurements of clouds in conjunction with flights of the University of North Dakota Citation research aircraft. One of the goals of this IOP was to validate ground-based retrievals of cloud microphysics using aircraft in situ measurements. The March 2000 cloud IOP was a very successful field experiment with a wide variety of cloud types observed during the three-week period. During the IOP, four low-level stratus cases (3, 17, 19, and 21 March) were intensively observed by the ground-based remote sensors and aircraft instruments resulting in a total of 10 h of simultaneous data from the two platforms. Three additional stratus cases during the IOP (14, 15, and 29 March) were analyzed for time periods when the aircraft was unavailable. When these additional results are combined with the retrievals from the four in situ cases, a total of 36 h of surface data are used to derive the empirical relationship between cloud-droplet effective radius and radar reflectivity.

Among the ground-based instrument suite, the MMCR is the centerpiece. The MMCR operates at a wavelength of 8 mm (35 GHz) in a vertically pointing mode, and provides continuous profiles of radar reflectivity of hydrometeors advecting through the radar field of view (Moran et al. 1998). The cloud-top height (Z_t) is derived from the cloud radar reflectivity profile, while cloud-base height (Z_b) is derived from a laser ceilometer. Because the radar is quite sensitive at these short ranges (~ -55 dBZ at 1 km), a few larger precipitation sized droplets that are insignificant to the overall water content and optical path can mask the actual cloud base. Since the laser ceilometer is sensitive to the second moment of the particle distribution instead of the sixth like the MMCR, the ceilometer provides a more faithful estimate of cloud base. The vertical resolutions of radar-derived cloud-top height and ceilometer-derived cloud-base height are 45 m and 8 m, respectively. The cloud LWP is retrieved from the microwave radiometer brightness temperatures measured at 23.8 and 31.4 GHz using a statistical retrieval method (Liljegren et al. 2001). The root-mean-square (rms) accuracies of the retrievals are about 20 g m^{-2} and 10% for cloud LWP below and above 200 g m^{-2}, respectively (Dong et al. 2000; Liljegren et al. 2001).

The University of North Dakota Citation research aircraft carried a number of Particle Measuring Systems (PMS) probes to provide in situ measurements of the cloud microphysical properties at a 4-Hz sampling rate. Cloud droplet spectra were measured with a PMS Forward Scattering Spectrometer Probe (FSSP-100) and were averaged to 1 Hz for this study. The FSSP probe sized and counted individual particles in 15 diameter bins, with bin centers from 4.4 to 52.3 μm. Corrections to particle concentrations have been applied to account for probe activity and coincidence (electronic dead time; Baumgardner et al. 1985) and for variations in the effective beam diameter (Dye and Baumgardner 1984). Corrections to particle sizes to account for electronic response time and beam inhomogeneity follow Baumgardner and Spowart (1990). The sizing correction scheme redistributes (re-bins) the counts, and the bin widths have been adjusted to account for ambiguities in the Mie scattering curve. LWC was calculated from each FSSP spectrum, and effective radius (r_e) was computed as the ratio of the third to the second moment of the cloud particle size spectrum.

Based on the previous studies (e.g., Baumgardner 1983; Dye and Baumgardner 1984; Baumgardner et al. 1985), Miles et al. (2000) summarized all possible errors for FSSP measurements. They are the following: 1) inhomogeneity across the length and width of the laser beam, which introduces sizing errors; 2) a limited response time in the detector electronic, which can lead to considerable underestimates of cloud-droplet number concentration (N); 3) coincident counts, which may underestimate N and overestimate r_e; 4) the propagation of error from particle concentrations and size to volume estimates, which can lead to large error to LWC; and 5) uncertainties associated with the calibration technique. The overall uncertainties in r_e, N, and LWC are 14%, 25%, and 30%, respectively, when all possible corrections are made to the measurements.

3. Methods

a. Profile of LWC

The microwave radiometer–derived cloud LWP and the MMCR-measured reflectivity profile are used to de-

rive the profile of cloud LWC. Following the development of F98 (see the appendix), the cloud LWC at a given range gate can be expressed as

$$\mathrm{LWC}(h) = \frac{\mathrm{LWP}}{\Delta h}\frac{Z^{1/2}(h)}{\sum_{\mathrm{base}}^{\mathrm{top}} Z^{1/2}(h)}, \quad (1)$$

where Δh is the radar range gate spacing (90 m in this study). The units of MMCR reflectivity $Z(h)$, LWP, and LWC are $\mathrm{mm}^6\ \mathrm{m}^{-3}$, $\mathrm{g\ m}^{-2}$, and $\mathrm{g\ m}^{-3}$, respectively. Equation (1) is identical to Eq. (9) of F98.

b. Profile of r_e: Reliance on solar transmission (M1)

The M1-inferred r_e profile is proportional to the layer-mean cloud-droplet effective radius derived as in D98 and to the ratio of the radar reflectivity to the integrated radar reflectivity. The cloud-base height obtained from the laser ceilometer is used to identify cloud base in the radar returns. D98 parameterized the retrieval process using the LWP, solar transmission, and cosine of solar zenith angle as

$$\overline{r_e} = -2.07 + 2.49\mathrm{LWP} + 10.25\gamma - 0.25\mu_0 + 20.28\mathrm{LWP}\gamma - 3.14\mathrm{LWP}\mu_0, \quad (2)$$

where the units of $\overline{r_e}$ and LWP are μm and 100 $\mathrm{g\ m}^{-2}$, respectively. Following the development of F95 and mathematical derivations, and collecting constant terms (see the appendix), we can write

$$r_e(h) = \overline{r_e}\left[\frac{\Delta H}{\Delta h}\frac{Z^{1/2}(h)}{\sum_{\mathrm{base}}^{\mathrm{top}} Z^{1/2}(h)}\right]^{1/3}, \quad (3)$$

where ΔH is cloud thickness (m)—the difference between the MMCR-derived cloud-top height and the ceilometer-derived cloud-base height. Our assumption of a single mode lognormal size distribution (see the appendix) should be also kept in mind since the retrieval results can be significantly affected by bimodal size distributions, such as when drizzle is present in the cloud layer. It is important to note that $r_e(h)$ derived from (3) is independent of the radar calibration similar to the independence shown by F98 in the LWC profile (1).

c. Profile of r_e: Solar transmission independent (M2)

During the night, or when optically thick cirrus or mid level clouds exist above low-level stratus clouds, and in broken stratus conditions, it is impossible to use the D98 technique to estimate the layer-mean cloud-droplet effective radius ($\overline{r_e}$) and to use M1 to estimate $r_e(h)$. To provide the cloud property estimates for these conditions, an empirical relationship between the effective radius $r_e(h)$ and radar reflectivity $\mathrm{dB}Z(h)$ can be defined.

To understand the physical meanings between $r_e(h)$ and $\mathrm{dB}Z(h)$, we take *10* $\log_{10}$ of both sides of (A1c) to change $Z(h)$ to $\mathrm{dB}Z(h)$. We obtain

$$10\ \log Z(h) = 10\ \log[2^6 10^{-12} N r_e^6(h)\ \exp(3\sigma_X^2)], \quad (4a)$$

which can be written

$$\mathrm{dB}Z(h) = 10[1.806 - 12 + 0.4343\ \ln N + 2.606\ \ln r_e(h) + 1.303\sigma_X^2]. \quad (4b)$$

Solving for $r_e(h)$,

$$r_e(h) = \frac{\exp(3.912 - 0.5\sigma_X^2)}{N^{0.167}}\exp[0.0384\mathrm{dB}Z(h)] = a\ \exp[0.0384\mathrm{dB}Z(h)]. \quad (4c)$$

As can be seen in (4c), there is reason to expect a well-defined functional relationship between $r_e(h)$ and $\mathrm{dB}Z(h)$ with the shape of the function governed by the exponential term. We find that the relationship between effective size and radar reflectivity is straightforward within the theoretical framework established above for vertically constant N and σ_X. However, from profile to profile, a may not necessarily remain constant but depends on the characteristics of the particle size distribution that are driven by such factors as cloud condensation nuclei (CCN) number and activity spectrum, updraft velocities and the water vapor supersaturation. Therefore, it is reasonable to assume that a will show some dependence on meteorological factors and perhaps on factors as diverse as the location of the airmass source region in the sense that it influences the nature of the CCN spectrum.

d. Sensitivity of r_e to the assumed vertically constant N and σ_X

To further explore the physical meanings of the constant a, consider Fig. 1. To produce Fig. 1, (4c) is used to assess the sensitivity of r_e to σ_X with fixed N(=200 cm^{-3}; Fig. 1a), and to N with fixed σ_X(=0.4; Fig. 1b). Figure 1 also includes the FSSP-measured effective radii plotted against the FSSP-calculated radar reflectivity to compare with the theoretical calculations from (4c). As Fig. 1b illustrates, the constant a does show a large variation from 15 to 24, and most of the FSSP-measured concentrations are between 50 and 800 cm^{-3} with fixed σ_X(=0.4). Figure 1 demonstrates that r_e is more sensitive (in an absolute sense) to the variation of radar reflectivity when the radar reflectivity is large. For example, from −60 to −30 dBZ, r_e only increases 4 μm from 2 to 6 μm (~ a factor of 3 increase), while r_e increases 14 μm from 6 to 20 μm (~ a factor of 3 increase, too) when the radar reflectivity increases from −30 to 0 dBZ. Figure 1 also suggests that the constant a and associated r_e are not a strong function of N and σ_X. For example, a varies by about 10% when σ_X is varied by ±0.2 from the fixed σ_X(=0.4; Fig. 1a), and about 12% when N is varied over a factor of 2 centered on 200 cm^{-3} (Fig. 1b). To examine the uncertainties of

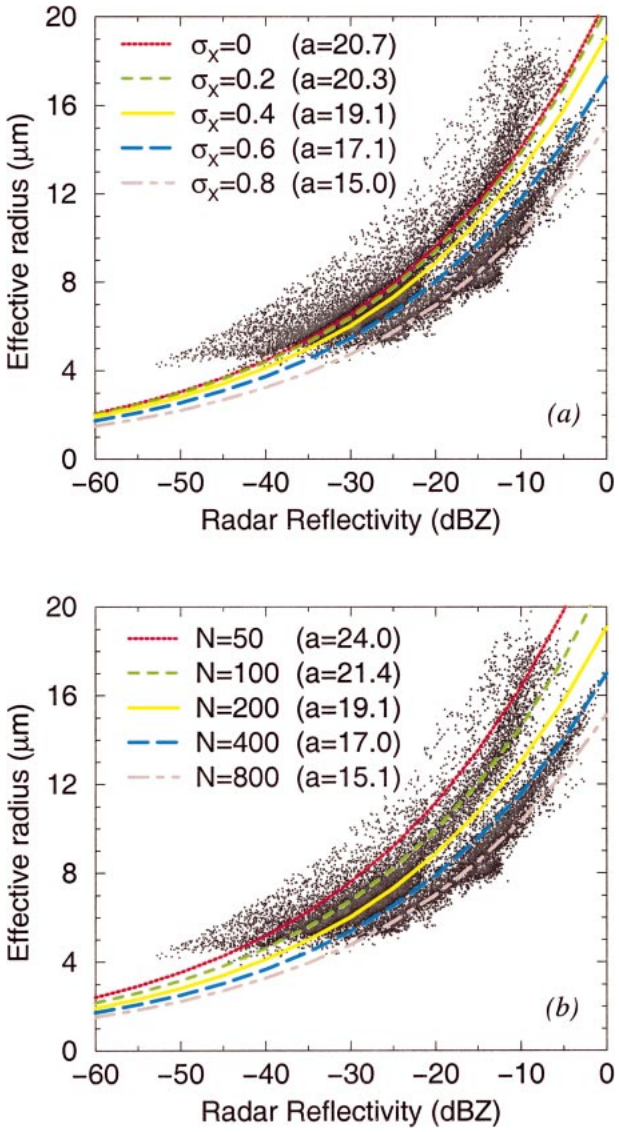

FIG. 1. Sensitivities (curves) of the surface-retrieved r_e to σ_x with (a) fixed $N = 200$ cm^{-3}, and (b) to N with fixed $\sigma_x = 0.4$. FSSP-measured effective radius vs FSSP-calculated radar reflectivity during the IOP (points).

both the M1 and M2 retrievals to the assumption of constant N and σ_X with height, eight profiles of N and σ_X from the 3 March aircraft data are used. The layer-mean values (standard deviations) of N and σ_X from these eight profiles, on average, are approximately 250 cm^{-3} (100 cm^{-3}) and 0.3 (0.05), which lead to the uncertainties of 9% and 2% to the r_e retrievals, respectively.

In an operational framework it is important to ensure that the assumptions under which these algorithms were derived are reasonable. To provide more accurate $\overline{r_e}$ values from D98 for the solar transmission-based M1, only low-level stratus clouds are selected that satisfy the following five criteria. They are 1) μ_0 is larger than 0.2, 2) the range of γ is 0.1 to 0.7, 3) LWP is between 20 and 600 g m^{-2}, 4) cloud-top height is less than 3 km, and 5) the range of radar reflectivity (dBZ) is -60 to 0. Justification for the first four criteria can be found in Dong et al. (2000).

The radar reflectivity is dominated by heavy drizzle droplets (median radius greater than 60 μm; F95) when the radar reflectivity is more than 0 dBZ. F95 and Mace and Sassen (2000) have demonstrated that light drizzle is frequently found when the radar reflectivity factor rises above -20 dBZ with a cumulative probability of $\sim$20% at 0 dBZ (Fig. 3 of F95). Between -20 and 0 dBZ, there is overlap between large cloud droplets and a precipitation mode composed of light drizzle. The presence of heavy drizzle (dBZ > 0) in clouds certainly influences the radar reflectivity measurements and the microwave radiometer brightness temperature. The existence of light drizzle also causes some additional bias in our retrievals, but this error is not always significant as proposed by Mace and Sassen (2000) and F95 as shown in Fig. 2. The FSSP is designed for measuring cloud droplets with a maximum mean radius of 26 μm (corresponding $r_e \sim 35$ μm). We find that volumes with a reflectivity factor near 0 dBZ correspond to effective radii of about 20 μm from both the surface and aircraft data in this study as shown in Fig. 2. Cloud droplets with radii smaller than 20 μm principally grow from water vapor condensation rather than collision coalescence (Duynkerke et al. 1995). The 2D-C probes, which are designed for measuring large particles, did not measure any large droplets during the four in situ cases.

4. Results and discussion

Four low-level stratus cases (3, 17, 19, and 21 March) were observed by ground-based remote sensors and aircraft instruments during the March 2000 cloud IOP at the ARM SGP site. Three additional stratus cases during the IOP (14, 15, and 29 March) were observed from the ground-based remote sensors only with a total of 36 h of data. Since the cloud temperatures of the four aircraft-supported cases were near or greater than 0°C, we assume that no ice was present in the clouds. The surface data have been averaged to 5-min resolution to have better correlations between the measurements and reasonable retrievals. The real sampling volumes from different surface instruments are dependent on their field-of-view angles, wind speed, and cloud-base height. To compare statistically the aircraft and surface results and to derive a representative empirical relationship between r_e and dBZ, a total of 10 h of aircraft data and 36 h of surface data during the IOP are used and plotted in Fig. 2. More detailed comparisons between the surface retrievals and aircraft FSSP data from two cases (3 and 21 March) are also discussed in this section.

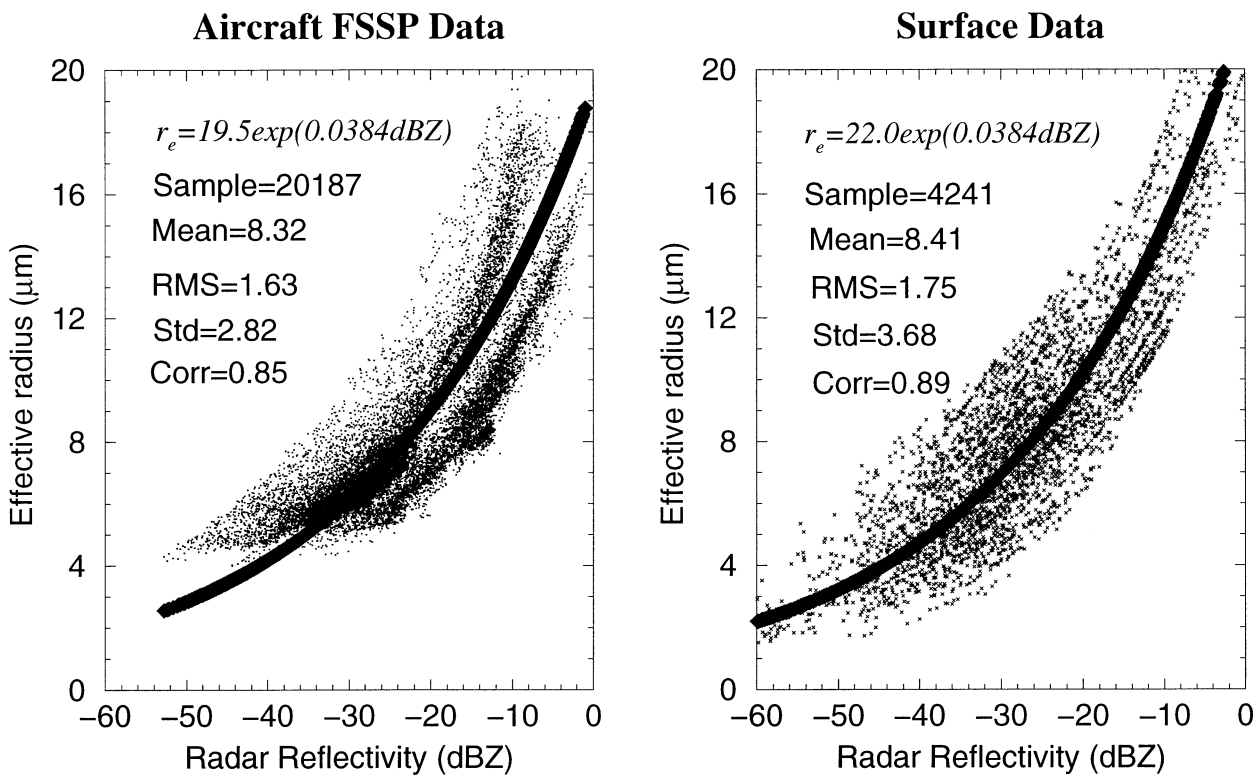

FIG. 2. 10 h of aircraft FSSP data at 1 Hz, and 36 h of surface data at 5-min resolution during the IOP. For the surface data, the points on the scatterplot are derived using M1 while the regression line is plotted using a best-fit value for $a = 22.0$ in (3c).

a. Empirical coefficients between r_e and dBZ from both the aircraft and surface data (M1)

The aircraft and surface M1-derived constants (a) between r_e and dBZ through a large number of samples are shown in Fig. 2 and their probability distribution functions (PDFs) are shown in Fig. 3. As Fig. 2 illustrated, the empirical constants derived from both the surface and aircraft FSSP data agree reasonably well during the IOP, their mean r_e values, rms differences, and correlation coefficients are nearly identical. The surface-derived mean and standard deviation of a (22.0 ± 5.2) are larger than those (19.5 ± 3.5) derived from the FSSP data but with a large range of overlap between them. The averaged value of radar reflectivity measured from the ground-based radar during the IOP is about 4 dBZ lower than that calculated from the FSSP data (Fig. 3), which may be due to either the sampling difference between the two datasets, the radar calibration, or calibration of the FSSP. As shown in Figs. 2 and 3, the FSSP sampled effective radii from ~ 4 μm with the minimum calculated reflectivity of -50 dBZ, while the surface radar reflectivity measurements started from -60 dBZ, this may be another reason to contribute the 4 dBZ lower surface mean reflectivity. The big advantage of M1 is to bypass radar calibration uncertainties, but it is strongly dependent on both the microwave radiometer–derived LWP and solar transmission. The similarity of the aircraft data and parameterization to the surface results and parameterization in Figs. 2–3 provides a qualitative evaluation of the surface retrievals. More detailed comparison between the aircraft and surface data in the following section will quantify the agreement between the two datasets.

b. Validation of the M1 and M2 results using the FSSP data on 3 and 21 March

On 3 March, with a northerly wind of ~ 15 m s^{-1} in the boundary layer, the aircraft remained within 20 km of the SGP central facility (SCF) flying a triangular pattern over several additional remote sites distributed in a small array northeast and east of the SCF. Early in the flight, the aircraft flew towards the SCF from the northeast, then slowly descended from cloud top to cloud base and quickly climbed back to cloud top in the triangle pattern. At around 1820 UTC, the aircraft flew northward from the SCF in the middle of cloud and returned to the SCF from the northeast at 1845 UTC. It then repeated the triangle pattern, used at the beginning of the flight, until 2000 UTC.

As shown in Fig. 4, the ceilometer-measured cloud base was near 0.5 km, while the radar-derived cloud-top height varied from 1 to 1.5 km during the 3-h period. The radar data were missing from 1830 to 1900 UTC.

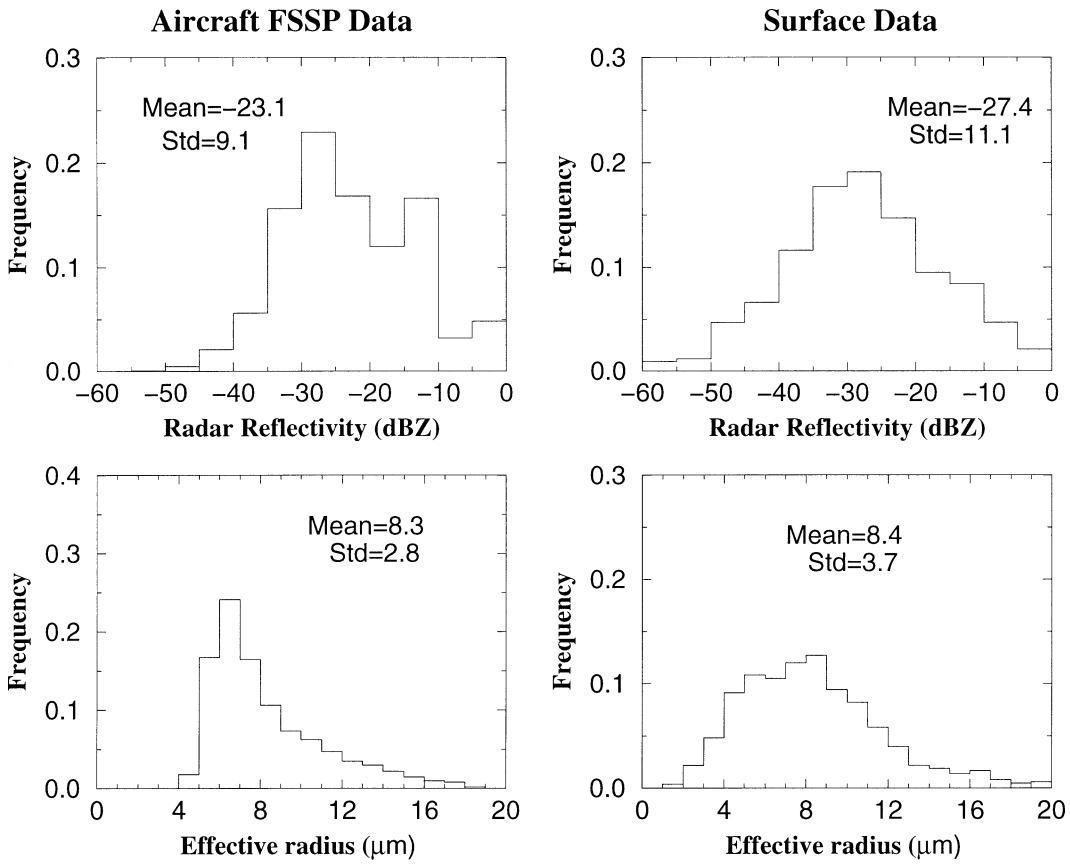

FIG. 3. PDFs of 10 h of FSSP data and 36 h of surface data (M1) during the IOP.

Overall, the surface-retrieved r_e values (5-min resolution) from both M1 and M2 (using the surface-derived constant $a = 22$ during the IOP) agree very well as shown in Figs. 4b–c, and they also have good agreement with the aircraft FSSP data (1-min resolution; Figs. 4d–e). The FSSP-derived LWC and r_e were averaged to 1-min resolution (corresponding to a length scale of roughly 5 km) to have the best match with the surface retrievals at each radar range gate. The surface retrievals (M1) in Figs. 4d–e were selected when they were at the same altitudes as the aircraft in the cloud (± 50 m). We note that this may not be a perfect match between the aircraft data and the surface retrievals because the aircraft did not always sample directly above the surface site. As demonstrated in Figs. 4d–e, the surface-retrieved LWC and r_e closely follow the trend of FSSP data, and PDFs (Fig. 6) from the available datasets in Figs. 4d–e also agree very well with the PDFs of FSSP data. Overall, the good agreement is encouraging, and suggests that both the FSSP data and the surface retrievals are capable of qualitatively characterizing similar cloud microphysics as a function of height and time (at 1-min resolution) during this cloud event.

The cloud properties on 21 March are similar to those observed in the 3 March case. The stratus cloud advected northward in a southerly flow at approximately of 10 m s^{-1}. The flight pattern of this case consisted primarily of ''S'' pattern flown over the SGP central facility and supplemental facilities within 20 km of the SCF. As shown in Fig. 5, there are apparently two quite different cloud layers, with very different cloud microphysics. The cloud base and top heights of the lower layer are around 0.5 and 1.5 km, respectively, at 1700 UTC. After 1730 UTC, the cloud-base height increased and cloud-top height remained nearly constant. By 1900 UTC, the lower layer merged with the upper layer. The cloud base and top heights of the upper layer are approximately 1.5 and 3 km, respectively, at 1700 UTC. This upper layer starts to break up at 1730 UTC. The base of the upper layer is gradually replaced or merged with the lower layer, while its top part forms a 100–200-m-thick layer at 1830 UTC. This thin upper layer is apparently the one sampled by the aircraft around 1900 UTC.

The LWC and r_e values of the upper layer are relatively uniform but much smaller than those from the lower layer as demonstrated in Fig. 5. The retrieved LWC and r_e profiles from the lower layer, which decrease with height, are very different from our conceptual model and should, therefore, challenge the validity of the algorithm. According to the cloud properties from both the surface retrievals and the aircraft FSSP data at

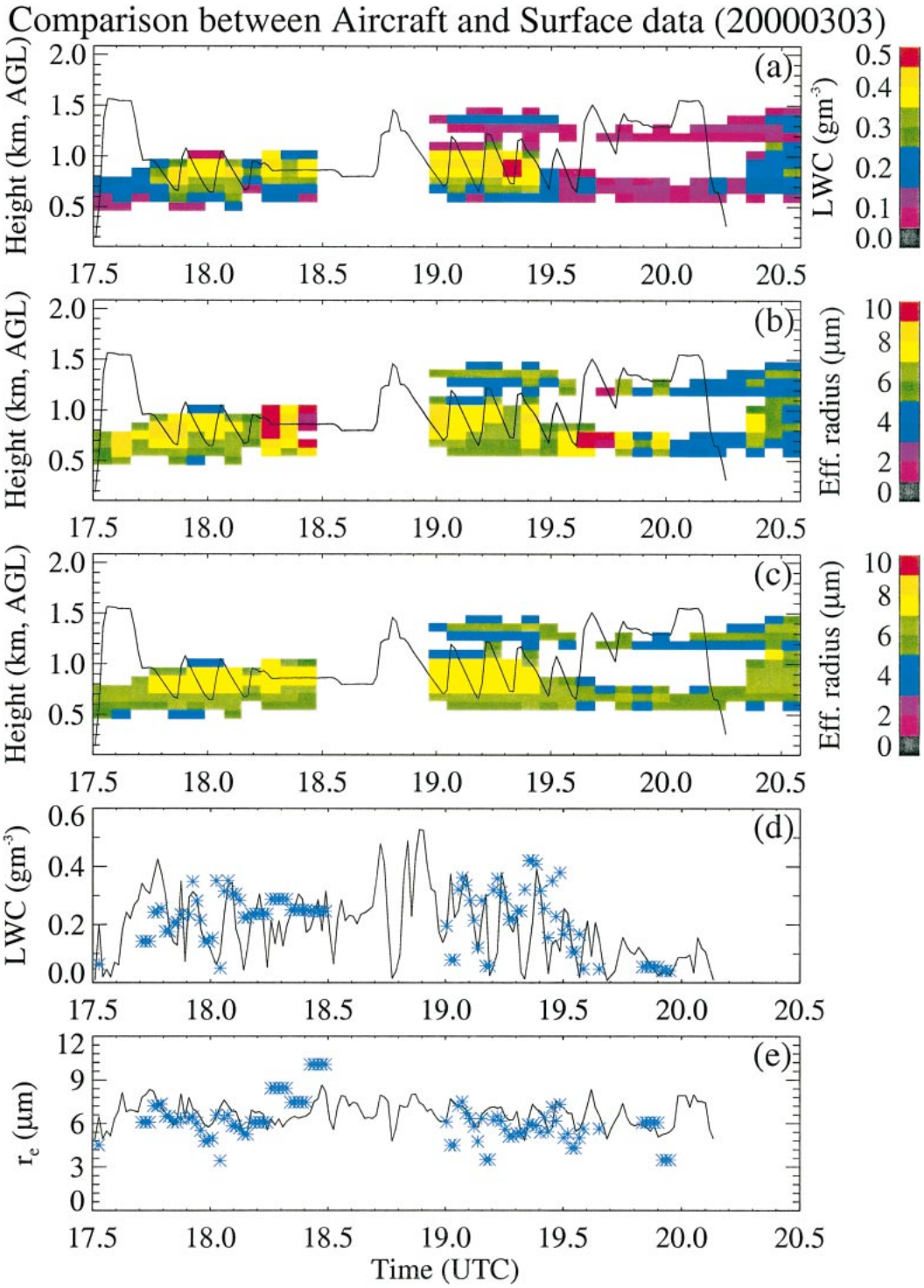

FIG. 4. (a) Cloud LWC and r_e profiles retrieved from (b) M1 and (c) M2 (5-min) and aircraft altitude (solid line) in the three upper panels. The 1-min averages of (d) cloud LWC and (e) r_e from the aircraft FSSP data (solid line) with corresponding surface retrievals from M1 (asterisks) at the same altitudes in the two lower panels.

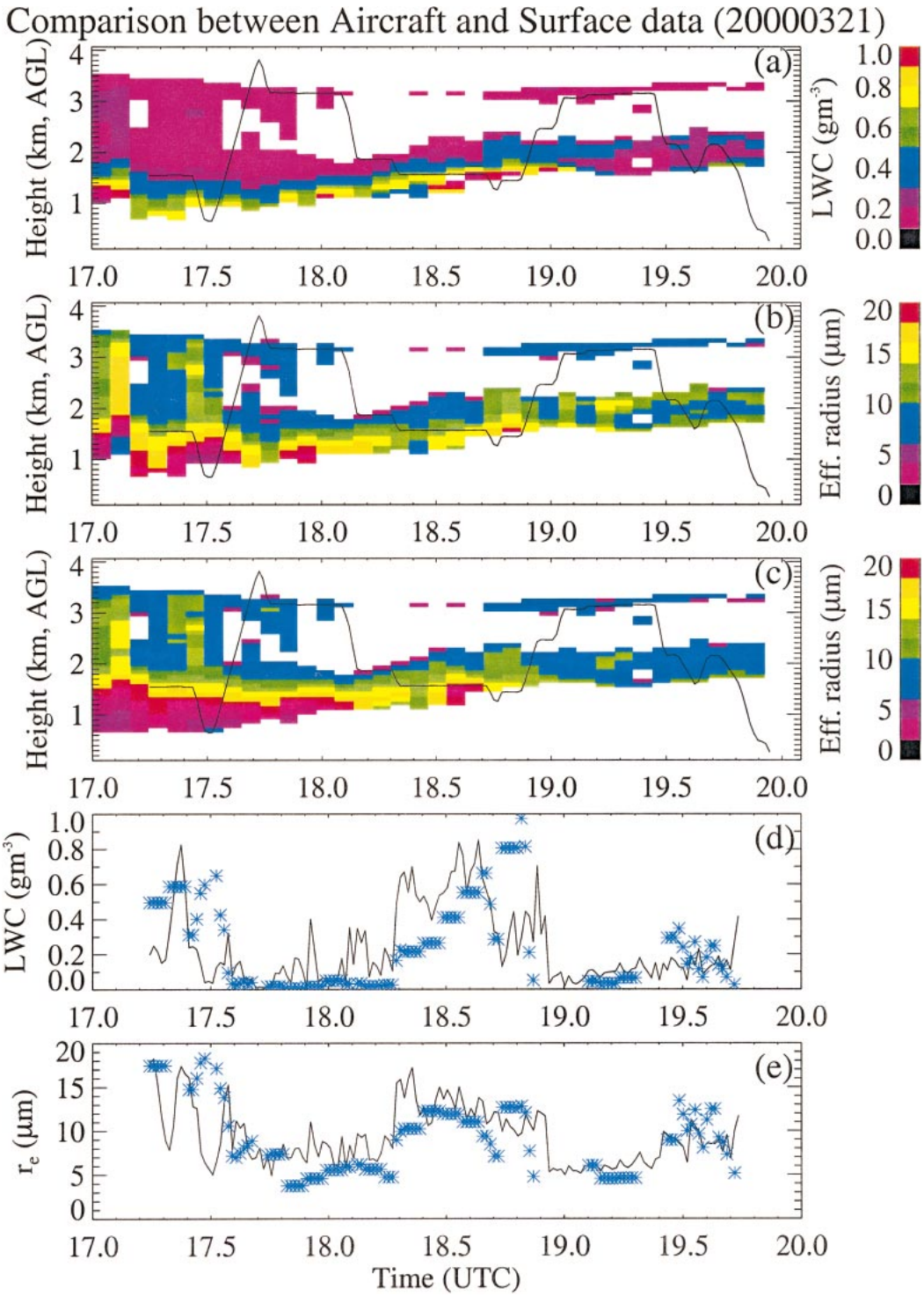

FIG. 5. Same as Fig. 4 but on 2 Mar.

the aircraft altitude in the cloud, we divide the 2.5-h flight time into five periods. The cloud microphysics from both period 1 (before 1730 UTC) and period 3 (from 1812 to 1854 UTC) represent the cloud properties of the lower layer with the large LWC and r_e values. The LWC and r_e from both period 2 (from 1730 to 1812 UTC) and period 4 (from 1854 to 1924 UTC) are much smaller than in the lower layer, and represent the cloud properties of the upper layer. The cloud properties from the last period (after 1924 UTC) represent the combi-

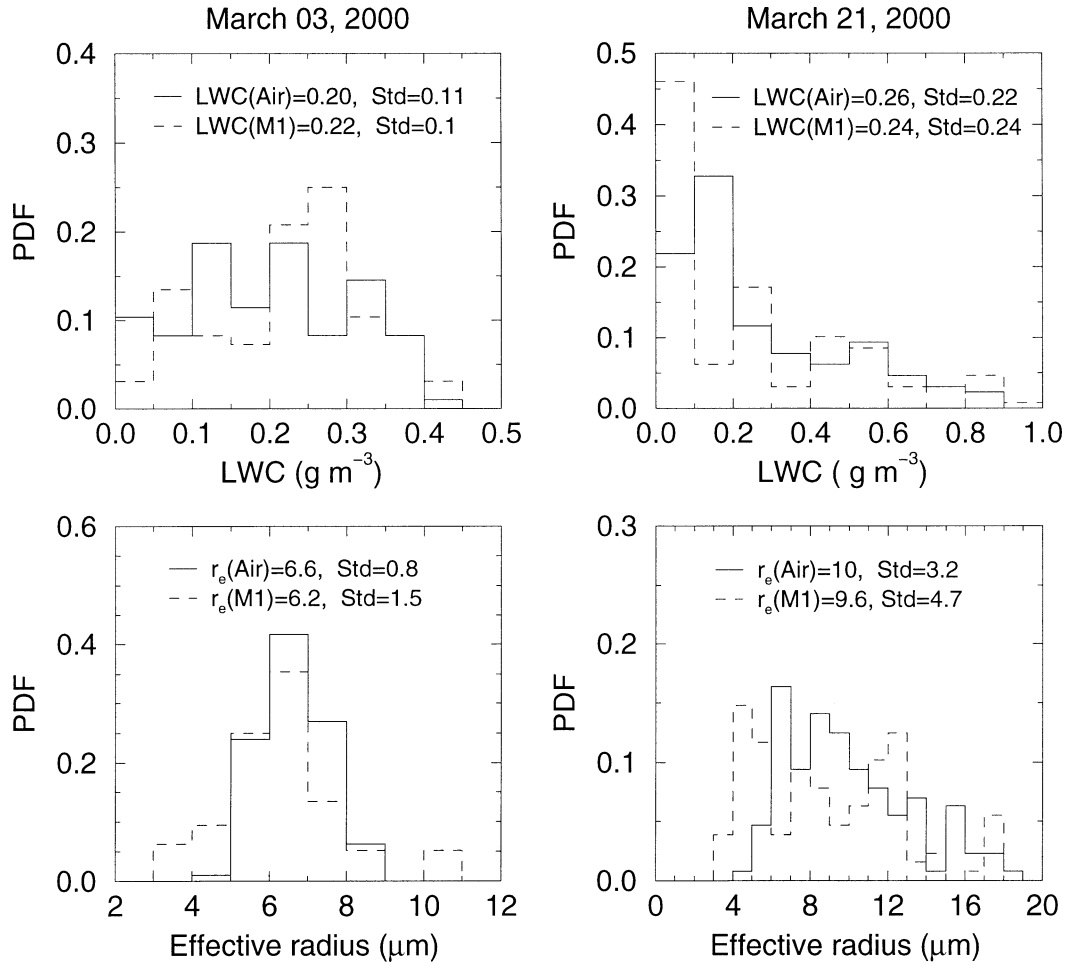

FIG. 6. PDFs of FSSP data (solid line) and surface retrievals (dashed line) from the available datasets in Figs. 4d–e and Figs. 5d–e.

nation of the lower and upper layers, and the cloud microphysical values are in between those of the lower and upper layers. The similarity in the PDFs of FSSP data and surface-derived cloud properties (M1), as well as the nearly identical means (Fig. 6), support the above discussion and suggest that the algorithm is able to accurately characterize cloud properties in circumstances that depart somewhat from the assumed well-mixed stratus-topped boundary layer. The totally different cloud microphysics between the lower and upper layers captured by both surface remote sensors and aircraft FSSP support our conclusion.

To quantify the agreement between the aircraft data and the surface retrievals from the above two cases, the 1-min datasets from Figs. 4d–e and Figs. 5d–e, and their 30-min averages are plotted in Fig. 7. Their corresponding mean values, standard deviations, and correlation coefficients are listed in Table 1. Figure 7 shows that the 1-min datasets are much more scattered than their 30-min averages, their standard deviations are larger, and their correlation coefficients are smaller than those from the 30-min averages as shown in Table 1. Furthermore, Table 1 also demonstrates that the standard deviations and correlation coefficients for the 15-min r_e averages are close to those from the 30-min r_e averages, and much different from those of the 1-min averages. While the standard deviations and correlation coefficients of the 15-min LWC averages are intermediate between the 1-min and 30-min averages. These results reveal that the standard deviations decrease and the correction coefficients increase with increased temporal averages, which is the same as the finding of D98 (Figs. 6 and 7 of Dong et al. 1998). We often assume that spatial and temporal statistics are essentially interchangeable. The 1-min datasets may be too short to test this approximation, given the huge mismatch in sample volumes. The evident agreement between the aircraft and surface data in the 30-min averages suggests that two platforms are reasonably capable of quantitatively characterizing the cloud microphysical properties of the cloud field over this temporal scale.

However, when we select only the 1-min aircraft data

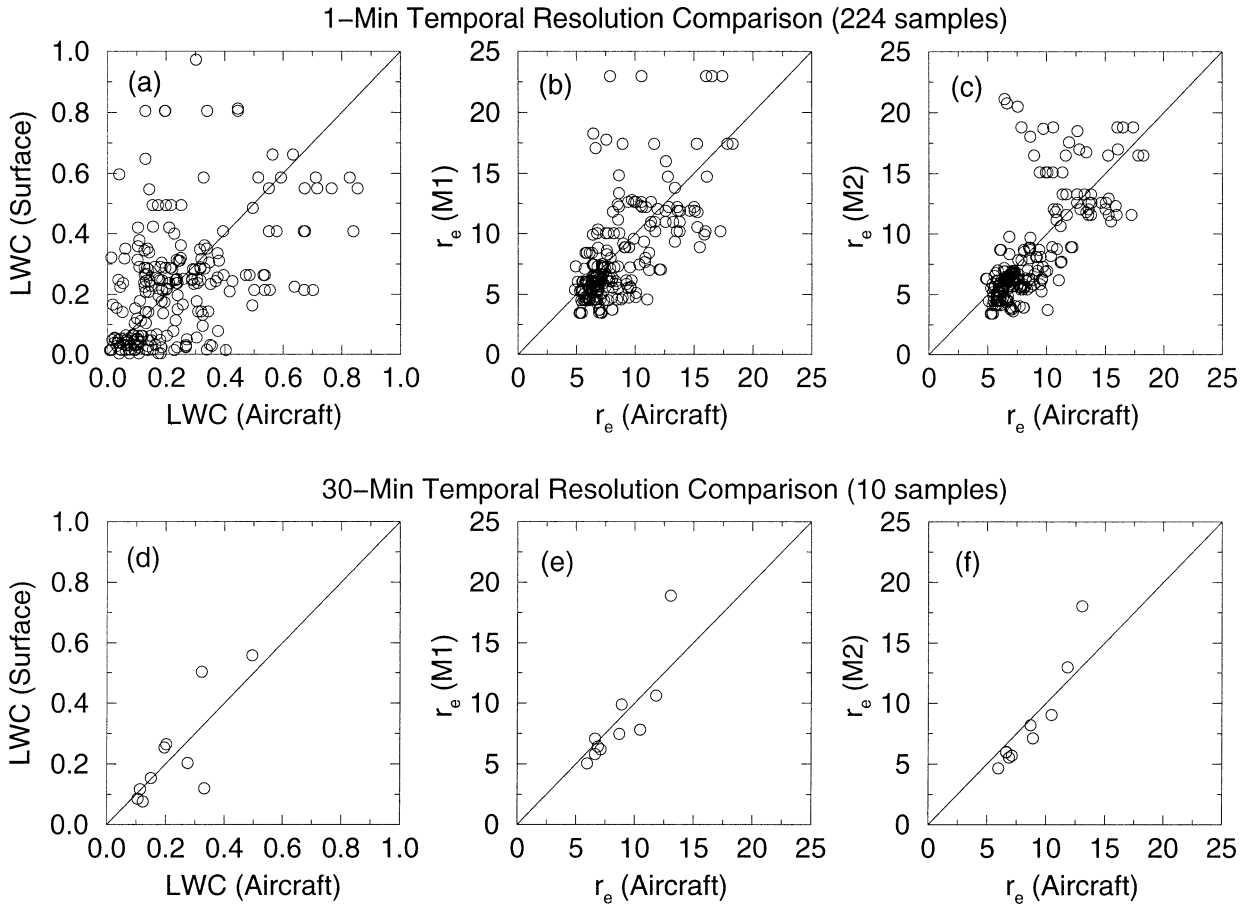

FIG. 7. Comparison of the surface retrievals from the two cases in Figs. 4 and 5 to the aircraft in situ measurements in (a)–(c) 1-min and (d)–(f) 30-min averages.

within 3 km of the surface site (the same time and altitudes as the surface retrievals), there are only 24 samples available from the original 224 samples and their standard deviations between the two datasets are larger and their correlation coefficients are smaller than all 1-min samples as shown in Table 1. This result suggests that restricting the comparison to the samples better matched in space and time between the surface and aircraft data does not result in a better comparison. There are several possible reasons that might cause this anomaly: 1) the sampling difference between two datasets, 2) too few samples to generate meaningful statistics, and/or 3) elements in the cloud field are much smaller than 3 km resulting in a total decorrelation in the cloud properties between the in situ and remotely sensed volumes. This finding is consistent with the comparison between surface and Geostationary Operational Environmental Satellite (GOES) results found from studies conducted using the 2000 IOP data (Dong et al. 2002) where a comparison of GOES 0.5° spatial averages with half-hourly averaged surface data results in good as or better comparison than using more closely

TABLE 1. The means and standard deviations (Std dev) of differences and correlation coefficients (Corr) of the surface retrievals relative to the aircraft in situ measurements on 3 and 21 Mar 2000. Numbers in parentheses are the samples for different temporal resolutions and the aircraft flew within 3 km of the surface site. Std dev is calculated from SQRT (rms^2 − mean^2), and rms and mean difference are in percent relative to the aircraft averages.

Temporal/ spatial resolution	LWC_{air} (g m^{-3})	LWC_{sfc}			$r_{e,air}$ (μm)	$r_{e,M1}$			$r_{e,M2}$		
		Mean (%)	Std dev (%)	Corr		Mean (%)	Std dev (%)	Corr	Mean (%)	Std dev (%)	Corr
1 min (224)	0.236	−2.5	84	0.47	8.52	−4.8	36.4	0.64	−4.7	34.6	0.70
15 min (16)	0.239	−0.42	59	0.62	8.46	−5.9	24.0	0.82	−3.5	23.6	0.90
30 min (10)	0.231	1.3	42.6	0.80	8.61	−1.0	25.5	0.86	−3.3	22.5	0.94
3 km (24)	0.222	23.4	113	0.32	8.81	13.1	51.4	0.27	28.3	60.7	0.34

matched data (i.e., a 3 × 3 GOES pixel array centered on the SCF compared to 5-min surface averages at the time of satellite image; Table 3 of Dong et al. 2002).

The huge sampling difference between the aircraft in situ and the surface measurements has been extensively discussed in D98. The surface retrieval technique uses data from a cylinder of cloud directly above the ground-based instruments. The microwave radiometer has a nominal field of view of 5°. At 1 km this translates into a horizontal diameter of 90 m. For a typical cloud thickness of 500 m, the instantaneous sample volume for microwave radiometer is about 3×10^6 m^3. The ground-based solar radiation measurement samples an even larger volume because of its hemispheric field of view. Given the aircraft speed of 85 ms^{-1} for low-level stratus operations during the IOP, the aircraft traveled about 5 km of distance in 1 min. The FSSP has a depth of field of about 3 mm and a beam diameter of 0.2 mm, giving a sample cross section of about 6×10^{-7} m^2 (Baumgardner 1983). Thus in 1 min the aircraft samples about 3×10^{-3} m^3 of air. Therefore, even if we restrict the comparison to the samples better matched in space and time, the surface and aircraft data still have a large sampling volume mismatch. Evidently, statistical intercomparisons of cloud properties will need to be performed until alternate means of in situ sampling are initiated.

5. Conclusions

Two methods have been discussed for inferring the profiles of cloud microphysics in boundary layer liquid or liquid dominant status. The first method (M1) uses measurements of cloud LWP and a profile of radar reflectivity together with a previously derived layer-mean cloud-droplet effective radius to infer the profiles of cloud liquid content and effective radius. This algorithm is independent of the radar calibration and is applicable to overcast low-level stratus clouds that occur during the day. In order to extend the conditions under which the algorithm can be applied, we describe a second method (M2) that uses an empirical relationship between effective radius and radar reflectivity based on theory and the results of method 1. To compare statistically the aircraft and surface data and to derive a representative empirical relationship between r_e and dBZ, a total of 10 h of aircraft data and 36 h of surface data during the IOP are used and show reasonable similarity (Figs. 2 and 3).

More detailed comparisons in Figs. 4–5 demonstrate reasonable agreement between the aircraft and surface data. To quantify the comparison between the aircraft data and the surface retrievals from these two cases, the 1-min datasets from Figs. 4d–e and Figs. 5d–e, and their 30-min averages are plotted in Fig. 7. Their corresponding mean values, standard deviations, and correlation coefficients (Table 1) show that the standard deviations decrease and the correlation coefficients increase with increased temporal averages (See also D98). The agreement between the aircraft and surface data in the 30-min averages suggests that two platforms are at least capable of characterizing the cloud microphysics over this temporal scale. However, when we select only the 1-min aircraft data within 3 km of the surface site at the same time and altitudes as the surface retrievals, the standard deviations of differences between the two datasets are larger and their correlation coefficients are smaller than all 1-min samples as shown in Table 1. This result suggests that restricting the comparison to the samples better matched in space and time does not result in a better comparison likely because of the huge sampling volume mismatch between the two datasets. This result also suggests that a statistical approach to validation is likely the most reasonable approach for this particular combination of clouds and data types.

These methods, combined with previously developed methods (D98), have been integrated into a single framework to provide the vertical profiles and layer-mean cloud microphysical properties of low-level stratus clouds; we apply method 1 during daytime and overcast low-level stratus clouds, and method 2 for other cloud conditions such as at night and during multiple layer situations. However, given the sensitivity of the constant a to the characteristics of the particle size distribution, the application of method 2 to other time periods and other sites should be done with caution.

Acknowledgments. The surface-based data were obtained from the Atmospheric Radiation Measurement (ARM) Program sponsored by the U.S. Department of Energy (DOE), Office of Energy Research, Office of health and Environmental Research, and Environmental Sciences Division. Special thanks to Ms. S. Benson for processing the surface data, Dr. J. Liljegren for reprocessing the ground-based microwave radiometer data, and Mr. M. Poellot for providing the aircraft FSSP data. During this study, the authors were supported by the ARM Program under Grant DE-AI02-97ER62341, NASA CERES Program under Contract NAG-1-2250, and NASA EOS validation program under Contract NAG-5-6458.

APPENDIX

Mathematical Derivations of Profiles of LWC and r_e (M1)

Assuming the cloud-droplet number concentration and lognormal size distribution are constant with height, and following the development of F95, we can express the radar reflectivity $Z(h)$ as

$$Z(h) = 2^6 N\langle r^6(h)\rangle = 2^6 N r_m^6(h) \exp(18\sigma_X^2), \quad \text{(A1a)}$$

where r_m is the median radius and σ_X is the logarithmic width of the size distribution. Using the fundamental expression for effective radius $r_e(h)$

$$r_e(h) = \frac{\langle r^3(h)\rangle}{\langle r^2(h)\rangle} = r_m(h)\,\exp(2.5\sigma_X^2), \qquad \text{(A1b)}$$

(A1a) can be written

$$Z(h) = 2^6\ 10^{-12}\ Nr_e^6(h)\,\exp(3\sigma_X^3). \qquad \text{(A1c)}$$

The units of $r_e(h)$, $Z(h)$, and N are μm, mm^6 m^{-3}, and cm^{-3}, respectively. The LWC at a given height can be expressed as

$$\mathrm{LWC}(h) = \frac{4}{3}\pi\rho_w Nr_e^3(h)\,\exp(-3\sigma_X^2), \qquad \text{(A2a)}$$

where ρ_w is the density of liquid water (10^6 g m^{-3}) and the unit of LWC(h) is g m^{-3}. Combining (A2a) with (A1c) by eliminating $r_e(h)$ and collecting constant terms yields

$$\mathrm{LWC}(h) = \frac{\pi}{6}\exp(-4.5\sigma_X^2)[NZ(h)]^{1/2}. \qquad \text{(A2b)}$$

The LWP equation can be similarly expressed as

$$\mathrm{LWP} = \frac{4\pi}{3}\rho_w N\overline{r_e^3}\,\exp(-3\sigma_X^2)\Delta H, \qquad \text{(A3a)}$$

or integrating (A2b) from cloud base to cloud top

$$\mathrm{LWP} = \sum_{\text{base}}^{\text{top}} \mathrm{LWC}(h)\Delta h$$

$$= \frac{\pi}{6}\exp(-4.5\sigma_X^2)N^{1/2}\Delta h \sum_{\text{base}}^{\text{top}} Z^{1/2}(h), \qquad \text{(A3b)}$$

where Δh is the radar range gate spacing (90 m in this study), ΔH is cloud thickness (m)—the difference between the MMCR-derived cloud-top height and the ceilometer-derived cloud-base height—and the unit of LWP is g m^{-2}. Solving for $N^{1/2}$ from (A3b) and substituting into (A2b), the LWC at a given range gate then becomes

$$\mathrm{LWC}(h) = \frac{\mathrm{LWP}}{\Delta h}\frac{Z^{1/2}(h)}{\sum_{\text{base}}^{\text{top}} Z^{1/2}(h)}. \qquad \text{(A4)}$$

Equation (A4) is identical to Eq. (9) of F98, but with more constraints, such as the range of LWP is from 20 to 600 g m^{-2}, and the radar reflectivity is between -60 and 0 dBZ. The cloud-droplet effective radius at a given range gate can be derived from (A2a)

$$r_e(h) = \left[\frac{\mathrm{LWC}(h)}{\frac{4\pi}{3}\rho_w N}\right]^{1/3}\exp(\sigma_X^2). \qquad \text{(A5a)}$$

Solving for N from (A3a) and substituting N and LWC(h) from (A4) into (A5a), and collecting constant terms, we can write

$$r_e(h) = \overline{r_e}\left[\frac{\Delta H}{\Delta h}\frac{Z^{1/2}(h)}{\sum_{\text{base}}^{\text{top}} Z^{1/2}(h)}\right]^{1/3}. \qquad \text{(A5b)}$$

REFERENCES

Baumgardner, D., 1983: An analysis and comparison of five water drop measuring instruments. *J. Climate Appl. Meteor.*, **22,** 891–910.

——, and M. Spowart, 1990: Evaluation of the Forward Scattering Spectrometer Probe. Part III: Time response and laser inhomogeneity limitations. *J. Atmos. Oceanic Technol.*, **7,** 666–7672.

——, W. Strapp, and J. E. Dye, 1985: Evaluation of the Forward Scattering Spectrometer Probe. Part II: Corrections for coincidence and dead-time losses. *J. Atmos. Oceanic Technol.*, **2,** 626–632.

Dong, X., T. P. Ackerman, E. E. Clothiaux, P. Pilewskie, and Y. Han, 1997: Microphysical and radiative properties of boundary layer stratiform clouds deduced from ground-based measurements. *J. Geophys. Res.,* **102,** 23 829–23 843.

——, ——, and ——, 1998: Parameterizations of microphysical and shortwave radiative properties of boundary layer stratus from ground-based measurements. *J. Geophys. Res.*, **103,** 31 681–31 693.

——, P. Minnis, T. P. Ackerman, E. E. Clothiaux, G. G. Mace, C. N. Long, and J. C. Liljegren, 2000: A 25-month database of stratus cloud properties generated from ground-based measurements at the ARM SGP site. *J. Geophys. Res.*, **105,** 4529–4537.

——, ——, G. G. Mace, W. L. Smith Jr., M. Poellot, R. Marchand, and A. Rapp, 2002: Comparison of stratus cloud properties deduced from surface, GOES, and aircraft data during the March 2000 ARM Cloud IOP. *J. Atmos. Sci.*, **59,** 3265–3284.

Duynkerke, P. G., H. Zhang, and P. J. Jonker, 1995: Microphysical and turbulent structure of nocturnal stratocumulus as observed during ASTEX. *J. Atmos. Sci.*, **52,** 2763–2777.

Dye, J. E., and D. Baumgardner, 1984: Evaluation of the Forward Scattering Spectrometer Probe. Part I: Electronic and optical studies. *J. Atmos. Oceanic Technol.*, **1,** 329–344.

Frisch, A., C. W. Fairall, and J. B. Snider, 1995: Measurement of stratus cloud and drizzle parameters in ASTEX with a K-band Doppler radar and a microwave radiometer. *J. Atmos. Sci.,* **52,** 2788–2799.

——, G. Feingold, C. W. Fairall, and T. Uttal, 1998: On cloud radar and microwave radiometer measurements of stratus cloud liquid water profiles. *J. Geophys. Res.*, **103,** 23 195–23 197.

Liljegren, J. C., E. E. Clothiaux, G. G. Mace, S. Kato, and X. Dong, 2001: A new retrieval for cloud liquid water path using a ground-based microwave radiometer and measurements of cloud temperature. *J. Geophys. Res.*, **106,** 14 485–14 500.

Mace, G. G., and K. Sassen, 2000: A constrained algorithm for retrieval of stratocumulus cloud properties using solar radiation, microwave radiometer, and millimeter cloud radar data. *J. Geophys. Res.*, **105,** 29 099–29 108.

Miles, N. L., J. Verlinde, and E. E. Clothiaux, 2000: Cloud-droplet size distributions in low-level stratiform clouds. *J. Atmos. Sci.*, **57,** 295–311.

Moran, K. P., B. E. Martner, M. J. Post, R. A. Kropfli, D. C. Welsh, and K. B. Widener, 1998: An unattended cloud-profiling radar for use in climate research. *Bull. Amer. Meteor. Soc.*, **79,** 443–455.

Stokes, G. M., and S. E. Schwartz, 1994: The Atmospheric Radiation Measurement (ARM) program: Programmatic background and design of the cloud and radiation testbed. *Bull. Amer. Meteor. Soc.,* **8,** 1251–1256.